ACS Sustainable Chemistry & Engineering

Research Article

pubs.acs.org/journal/ascecg

Bioinspired Ultrastable Lignin Cathode via Graphene Reconfiguration for Energy Storage

Xiumei Geng,[†,§] Yelong Zhang,[†,§] Li Jiao,[†,§] Lei Yang,[†] Jonathan Hamel,[†] Nicola Giummarella,[‡] Gunnar Henriksson,[‡] Liming Zhang,[‡] and Hongli Zhu*[,†]

[†]Department of Mechanical and Industrial Engineering, Northeastern University, 360 Huntington Avenue, Boston, Massachusetts 02115, United States

[‡]Division of Wood Chemistry and Pulp Technology, Department of Fiber and Polymer Technology, Royal Institute of Technology, KTH, 114 28, Stockholm, Sweden

Supporting Information

ABSTRACT: Lignin extracted from trees is one of the most abundant biopolymers on Earth. Quinone, a substructure in lignin, can be used for energy storage via reversible redox reactions through absorbing and releasing electrons and protons. However, these efforts have encountered hindrances, such as short life cycle, low cycling efficiency, and a high self-discharge rate. All of these issues are related to electrode dissolution by electrolyte solvents and the insulating nature of lignin. Addressing these critical challenges, for the first time, we use a reconfigurable and hierarchical graphene cage to capture the lignin by mimicking the prey-trapping of venus flytraps. The reconfigurable graphene confines the lignin within the electrode to prevent dissolution, while acting as a three-dimensional current collector to provide efficient electron transport pathways during the electrochemical reaction. This bioinspired design enables the best cycling performance of lignin reported so far at 88% capacitance retention for 15 000 cycles and 211 F/g capacitance at a current density of 1.0 A/g. This study demonstrates a feasible and effective strategy for solving the long-term cycling difficulties of lignin-based electrochemically active species and makes it possible to utilize lignin as an efficient, cheap, and renewable energy storage material.

KEYWORDS: *Lignin, Charge transfer, Graphene reconfiguration, Pseudocapacitor, Bioinspired*

INTRODUCTION

There has been a steady increase in demand for clean and efficient energy storage materials due to ever rising concerns about limited global fossil fuel reserves, environmental consequences of combustion, and associated climate change. Lignin is one of the most abundant natural biopolymers on Earth, which comprises approximately 15−25 wt % of wood. It can be obtained as a byproduct from chemical pulping and biofuel production processes[1,2] either in the form of the valuable dispersing agent lignosulfonate or as kraft lignin, which nowadays is mainly burned as fuel during the chemical recovery process of kraft pulping. Chemically, lignin is a polymer constituted by hydroxyphenylpropane units connected with each other by ethers or by carbon−carbon bonds with a heterogeneous structure.[3−5] Two kinds of technical lignin are available: (1) lignosulfonate and (2) alkali lignin. The former is a water-soluble derivate obtained as a byproduct of the sulfite pulping process and is used as a dispersing agent in concrete and other materials. The latter is obtained as byproducts from alkaline pulping—soda, anthraquinone, and kraft pulping processes.[6,7] The alkaline lignin could easily be extracted as a byproduct,[8] however, it has been difficult to develop a commercially feasible application for it. 50 million tons of lignin is produced annually from the pulp and paper industries, but only 1−2% of lignin is isolated from black liquors and used for specialty products.[8,9] Lignin valorization offers the possibility to provide potential high-value products, such as highly functional monomer and oligomer products in the chemical and pharmaceutical industries.[10] Therefore, there are substantial environmental and economic benefits in exploring a valuable application of this large amount and underutilized material from nature.

Recently, lignin-based materials have been actively explored for their applications in energy storage and conversation.[11−18] Usually lignin was first carbonized at high temperature over 1000 °C, then the resultant carbonaceous remnant was used as electrodes of batteries and supercapacitors. However, the whole process involves high energy consumption and low yield, usually <10%. Inganäs used the conjunction of lignin and polypyrrole as a cathode electrode, in which the quinone group reversibly accepts and releases electrons and protons during

Received: February 1, 2017
Published: February 16, 2017

DOI: 10.1021/acssuschemeng.7b00322
ACS Sustainable Chem. Eng. XXXX, XXX, XXX−XXX

charge/discharge cycles.[1] But there are two key challenges to directly use lignin for energy storage: (1) Lignin possesses extremely low electric conductivity. Thus most of its potentially active sites are electrochemically inaccessible. (2) Ligninsulfonate can readily dissolve in aqueous media, which would cause a steady loss of active materials in an electrochemical device. Numerous efforts were made to increase the conductivity of lignin by combing it with various conductive polymers such as polypyrrole used in Inganäs's work, but since the conductive polymer is unstable during electrochemical charge/discharge, the lignin/polypyrrole-based electrode still exhibits poor cycling stability.

Bioinspiration, resorting to inspirations from structures and functions found in natural materials, is an effective methodology to design more reliable, efficient, and environmentally friendly materials or structures. Venus flytraps capture prey through mobile leaves acting as traps. Inspired by this carnivorous plant, we used a reconfiguration graphene that can "open" and "close" to capture and confine lignin within the conductive graphene matrix. Graphene is well-known for its high theoretical specific area, high electrical conductivity, high mechanical strength, as well as a low fabrication cost.[19−24] Herein, a venus flytraplike graphene was designed to act as a lignin host. The venus flytraplike graphene was kept high expansion in solution, while it was restacking under dry condition due to the van der Wals force between the adjacent layers of graphene. Lignin was trapped and wrapped in the expansion state of pristine few layer graphene in solution. The graphite−$FeCl_3$ was obtained by heating the graphite and anhydrous ferric chloride in a two-zone reactive container. The ferric chloride is intercalated between the graphite layers. Then, the hydrogen peroxide was added into the graphite−$FeCl_3$. In this process, a large amount of oxygen is produced, leading to the exfoliation of graphite to graphene. The reaction equation between $FeCl_3$ and H_2O_2 is proposed as follows:[25]

$$FeCl_3 + H_2O_2 \rightarrow FeCl_2 + H_2O + O_2$$

Here, graphene was used to capture and confine the lignin inside the cage, meanwhile provided efficient electron transfer pathways during electrochemical reactions. This would simultaneously resolve two hindrances for the electrochemical reversibility of lignin, i.e., poor electric conductivity and high solubility in aqueous media. The restacking graphene structure can provide effective space during the electrochemical reaction. Therefore, the graphene−lignin cathode shows good electrochemical rate performance and cycling stability. The capacity retention of the obtained lignin is 88% after 15 000 cycles at a current density of 2.0 A/g. Lignin presented the highest cycling stability for energy storage. Additionally, the conductive graphene provides efficient electron transfer pathways to enable pseudocapacitance retention at a good rate performance with 211 F/g under a current density of 1.0 A/g. These encouraging results pave the way to use sustainable and earth-abundant lignin for low-cost energy storage with good performance.

RESULTS AND DISCUSSION

Lignin is the second most abundant polymer on earth, composing 15−25% of wood, Figure 1a. A waste-to-energy strategy is enabled by the graphene-reconfiguration mechanism, and an earth-abundant and low-cost biopolymer is thus converted to an electron storage material, where the quinone functionalities are used for electron and proton storage and exchange during cycling. The two intrinsic problems of lignin, i.e., poor conductivity and dissolution by aqueous electrolytes, cause poor cycle life, low specific capacity, and low energy efficiency.

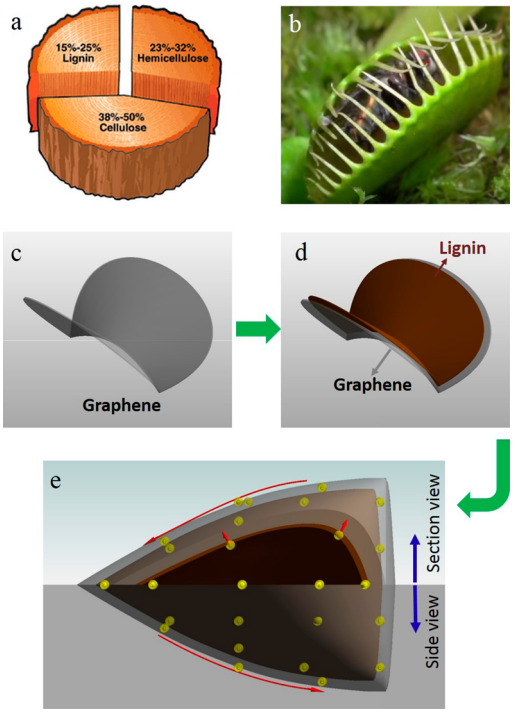

Figure 1. (a) Schematic of lignin composition in the wood. (b) Photograph of a venus flytrap plant. (c) Schematic of graphene made from interlayer catalytic exfoliation. (d) Graphene with open mouth trapping lignin. (e) Illustration of electron transportation in this hybrid material of graphene and lignin. Electrons are generated during electrochemical reaction and transferred from lignin to graphene.

In nature, as shown in Figure 1b, the leaves of the venus flytrap divide into two mobile halves. When prey lands inside the open leaves, the two halves close and imprison the plant's prey. In order to resolve the poor electronic conductivity and solubility issues of lignin, we designed the reconfigurable graphene to mimic the motion of the leaves of the venus flytrap. As a two-dimensional conductor with high surface area, good chemical stability, and excellent mechanical strength and flexibility, graphene is a useful growth substrate that can anchor diversified active materials for electrochemical applications. We mimic the mechanism of the venus flytrap trapping prey to capture and confine lignin inside a graphene cage, which is made possible by the reconfiguration behavior of graphene in wet and dry environments. The graphene opens in solvent as shown in Figure 1c, since we exfoliate bulk graphite to interconnected but open graphene structures via an interlayer catalytic exfoliation technique, as described below. One thin layer of lignin, shown in brown in Figure 1d, is deposited on the graphene surface through a physical adsorption process. The solvent is then removed, which causes the graphene to close. The $\pi-\pi$ interactions between the graphene sheets contribute to the formation of stable cages. During this capture process, the reconfigurable graphene functions as the carnivorous leaves of a flytrap, and the lignin as prey caught by the mobile graphene leaves. The interaction of graphene and lignin can be firmly ascribed to the noncovalent strong $\pi-\pi$ interaction because there are a large number of aromatic rings in lignin. As shown in Figure 1e side

DOI: 10.1021/acssuschemeng.7b00322
ACS Sustainable Chem. Eng. XXXX, XXX, XXX−XXX

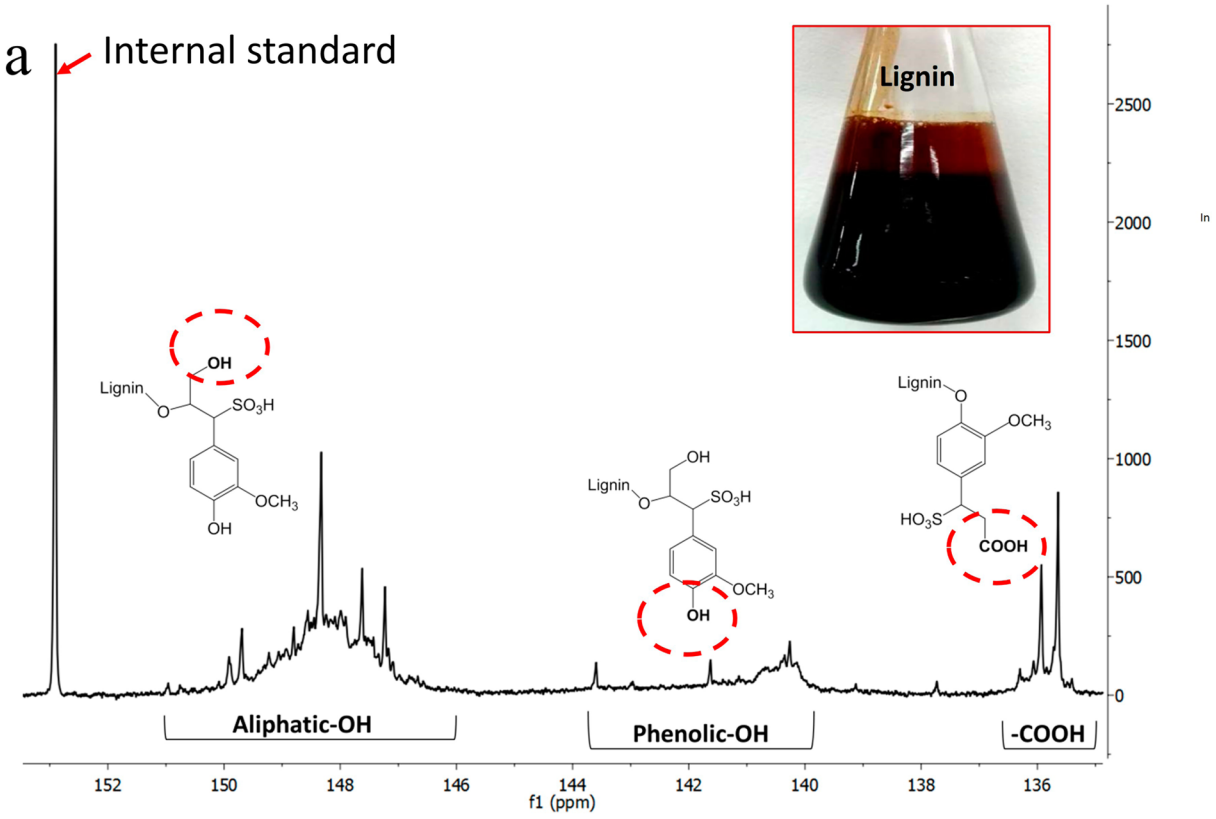

Table 1Variations of –OH group content in lignosulfonate according to the NMR test

	Aliphatic -OH	Phenolic	Carboxyl -OH
	(mmol/g)	(mmol/g)	(mmol/g)
Lignosulfonate	3.44	1.05	0.66
Lignosulfonate duplicate	3.47	1.17	0.68

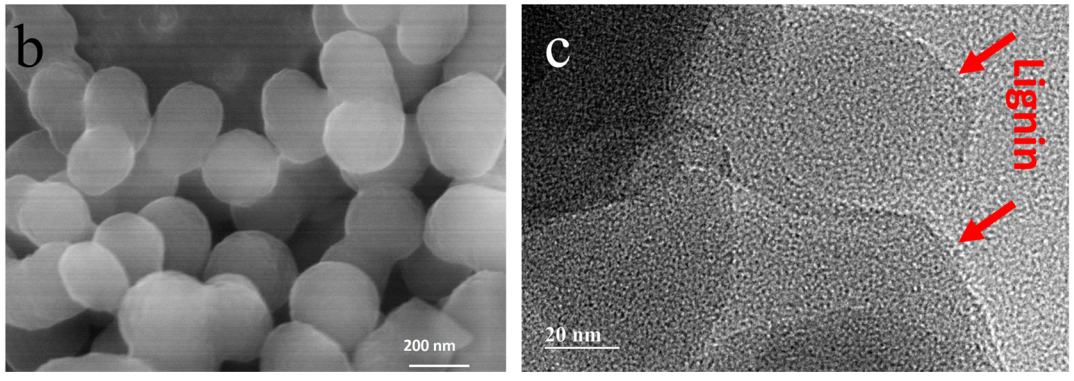

Figure 2. Structural characterization of lignin. (a) NMR spectra. (inset) Lignin solution in water showing ligninsulfonate suspension with 10 mg/mL. (b) SEM image showing spherical lignin. The lignin size is around 150 nm. (c) High magnification transmission electron microscopy image of lignin.

view, the lignin is trapped and confined inside the graphene cage, which is able to provide efficient electron transfer pathways. The yellow dots in Figure 1e section view therein represent electrons released from lignin during the charging process. The red arrows display the electron transfer from lignin to graphene and further transport to the external circuit to perform work. Graphene functions as a current collector simultaneously.

In recent years, the chemical structure of kraft lignin has been thoroughly studied by nuclear magnetic resonance (NMR) techniques,[26,27] while little attention has been paid to the chemical structure of lignosulfonate. It is generally more difficult to study the chemical structure of the latter than other types of lignin because of its poor solubility in organic solvents. Previous studies have shown lignosulfonate as a complex of sulfonated lignin polymers with a wide range of different molecular sizes.[28,29] According to the NMR spectra obtained in this study, Figure 2a, the lignosulfonate sample used in the present work contained a phenol group in the range of 1.05–1.17 mmol/g, Table S1. The corresponding NMR mapping

DOI: 10.1021/acssuschemeng.7b00322
ACS Sustainable Chem. Eng. XXXX, XXX, XXX−XXX

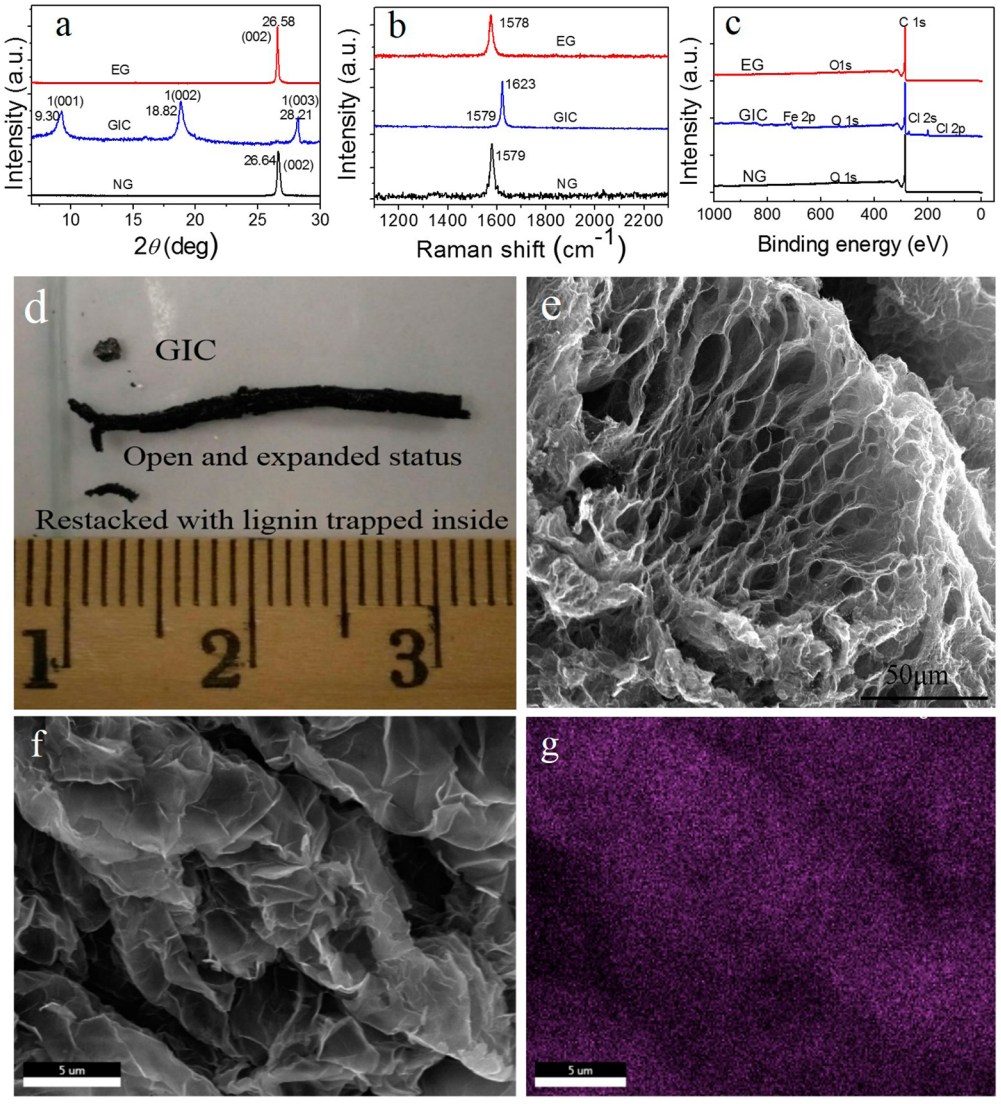

Figure 3. Structure and morphology of graphene and lignosulfonate−graphene composites. (a) XRD spectra of the NG, the GIC, and the EG, showing complete recovery of the graphite structure and the stage-1 GIC determined by an identity period of 9.37 Å. (b) Raman spectra of the NG, the GIC, and the EG. The high quality of EG is shown by the spectra comparison between EG and NG. (c) XPS spectra of the NG, the GIC, and the EG, showing the effective removals of the intercalated elements. (d) Pictures of GIC (without lignin), wet EG (without lignin), and dry EG (with lignin). (e) SEM image of EG after freeze-drying. (f) SEM image of EG with lignin under 100 °C for 1 h. (g) EDX mapping of sulfur present on the lignosulfonate polymer in the EG−lignin composite. The sample was prepared with blade cutting in liquid nitrogen.

signal of lignosulfonate is shown in Figure S1. The inset image shows ligninsulfonate suspension with 10 mg/mL in water. According to the gel permeation chromatography (GPC) test, the molecular weight of this lignosulfonate is around 4000 g/mol, Table S1. In pulping mills, the original complex lignin chain is broken into small molecules during the digestion process. The structure can potentially expose active groups in lignin and benefit the electrochemical utilization. Figure 2b shows the spherical morphology of lignin with a diameter approximately 150 nm. The high resolution TEM image, Figure 2c, indicated the amorphous nature of lignin.

The evolution and the quality of the natural graphite (NG), the graphite intercalated compound (GIC), and the exfoliated graphite (EG) are determined by the X-ray diffraction (XRD), Raman, and X-ray photoelectron spectroscopy (XPS) (Figure 3a−c), respectively. The single stage-1 $FeCl_3$ GIC has been obtained and identified by the three specific XRD peaks (Figure 3a). The intercalation is nearly complete with negligible residual nonintercalated graphite flakes. The high quality and purity of the EG are determined by the recovering of a single (002) peak and the absence of other impurity peaks upon thermal expansion. The EG peak (26.58) is shifted slightly from the pristine graphite (26.64), which is ascribed to the increasing interlayer spacing of the graphene sheet in the bulk EG. The high quality of the EG is further confirmed by the comparisons of Raman spectra of the EG and the NG (Figure 3b). The D peak of the EG is almost invisible, which is similar to the NG and quite different from general graphene oxide which has a prominent D peak.[30−34] The Raman spectroscopy of the GIC is consistent with that of the stage-1 $FeCl_3$-based bulk GIC.[35] The peak at 1623 cm^{-1} and a minimal-intensity G peak at 1579 cm^{-1} of the GIC suggest complete stage-1 intercalation. In order to verify removal of the Cl and Fe elements, XPS measurements are performed on the NG, the GIC, and the EG. The C 1s peak at ∼284.5 eV, associated with C−C bonds, was used as a reference. The small amount of oxygen in the XPS

DOI: 10.1021/acssuschemeng.7b00322
ACS Sustainable Chem. Eng. XXXX, XXX, XXX−XXX

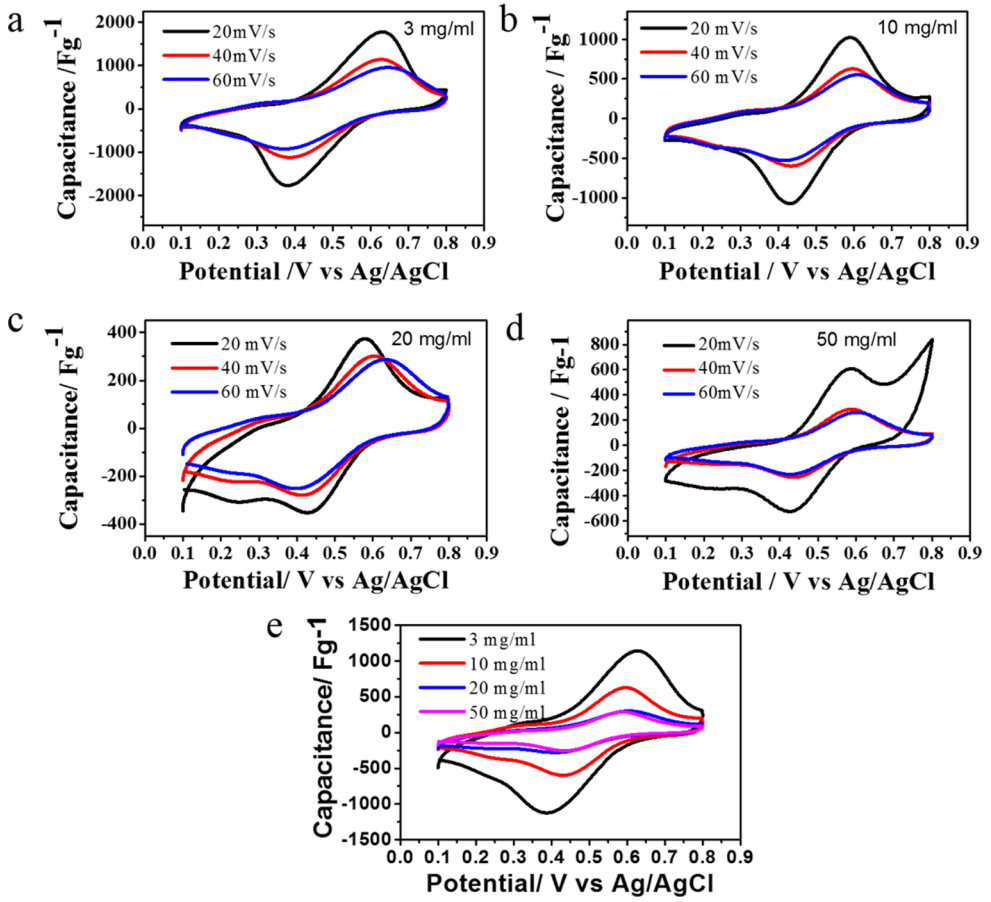

Figure 4. Cyclic voltammetric (CV) profiles of the graphene−lignosulfonate electrode with different mass loadings at different scan rates. (a) 3 mg/mL lignin solution at scan rates of 20, 40, and 60 mV/s. (b) 10 mg/mL lignin solution at scan rates of 20, 40, and 60 mV/s. (c) 20 mg/mL lignin solution at scan rates of 20, 40, and 60 mV/s. (d) 50 mg/mL lignin solution at scan rates of 20, 40, and 60 mV/s. (e) Comparison of 3, 10, 20, and 50 mg/mL lignin solutions at a scan rate of 40 mV/s.

originates from absorbed water vapor existing in the NG, the GIC, and the EG. We observe the peaks of Cl 2s, Cl 2p, and Fe 2p in XPS of the GIC (Figure 3c) in the form of Fe−Cl bond,[36] while Fe 2p, Cl 2s, and Cl 2p peaks of the EG almost disappear. A very small amount of residual Cl element remains as ∼0.08 atom % in the form of C−Cl bond. It should be noted that the resultant EG is low cost since we just used 30% H_2O_2, $FeCl_3$, and inexpensive graphite as raw materials. Meanwhile, the chemical process is facile and occurs in an environmentally friendly way. The rough cost of EG is estimated to be around 5 cents per gram according to this procedure.[37] A comparison of GIC, wet EG without lignin (corresponding SEM image presented in Figure 3e), and dry EG with lignin (corresponding SEM image presented in Figure 3f) is displayed in Figure 3d. We found the volume of dry EG with lignin becomes very small after water being removed between the graphene layers. This result indicates $\pi-\pi$ stacking occurs, which restacks the graphene layer together, and suggests that lignin is trapped between the graphene layers. Thus, a desired hierarchy results with conductive graphene layers covering the insulating but electrochemically active lignin, which provides redox pseudocapacitance. The morphology of the prepared graphene layers at open status is shown in Figure 3e by using freezing dry technique to maintain the structure. Figure S2 further present the open status of graphene. The special structure can be maintained in solution since the solvent works as a separator and prevents the van der Waals force between adjacent layers of graphene from assembling the stacks. These graphene layers are separated but they are connected at some points simultaneously. As a result graphene within this structure has high conductivity due to its intrinsic electric properties. This particular hierarchical structure allows other molecular and smaller size materials like lignin to penetrate into the relatively large honeycomb shape of the interconnected graphene matrix, which forms a uniform graphene and lignin composite. An image of these results is displayed in Figure 3f and sulfur mapping in Figure 3g shows uniform lignin distribution covering the surface of graphene layers.

The electrochemical performance of lignosulfonate−graphene composites are evaluated using three electrode cells in aqueous electrolyte with 0.1 M $HClO_4$, where the composite material is coated on platinum mesh as the working electrode, with platinum sheet and saturated Ag/AgCl as the counter and reference electrodes, respectively. Figure 4a shows the cyclic voltammetry (CV) profiles of the lignosulfonate electrode. There is a sharp oxidation peak at ∼0.6 V and an obvious reduction peak at ∼0.4 V, ascribing to the reduction and oxidation of the quinone groups on the lignosulfonate.[1] The reversible faradic reaction is illustrated in eq 1 as the protonation of two quinone functionalities, each of which are accepting one electron during the discharging process and losing one during the charging process.

In this reversible quinone/hydroquinone conversion, lignin can store and release two electrons and protons. As the

DOI: 10.1021/acssuschemeng.7b00322
ACS Sustainable Chem. Eng. XXXX, XXX, XXX−XXX

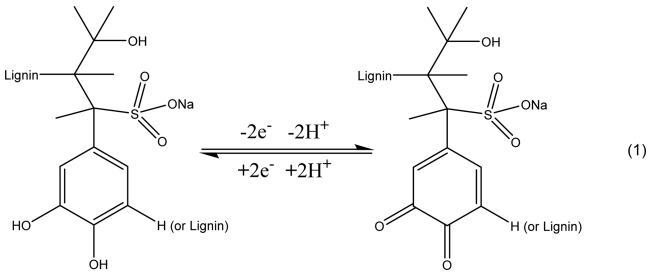

(1)

potential scan rate is increased from 20 to 60 mV/s, the current is increased proportionally, indicative of an ion-adsorption dependent redox processes.

The maximum capacitance is achieved at a 20 mV/s scan rate for lignosulfonate composites prepared in 3 mg/mL lignosulfonate solution. Typical CVs from pure graphene at the scan rates of 10−100 mV/s in $HClO_4$ are also shown for comparison (Figure S3). Specific capacitances of the samples are calculated using the voltammetric charge integration (cathodic current) from the cyclic voltammogram curves and considering the equation $C_S = Q/\Delta Em$ where C_S is the specific capacitance (F/g), Q is the charge of cathodic current (C), ΔE is the potential window (V), and m is the mass of the active material (g). The variations of specific capacitance values with scan rate for the pure graphene are given in Table S2. From the CV measurements, it is clear that at a scan rate of 20 mV/s, the highest specific capacitance exhibited by lignosulfonate composites is 138.4 F/g, whereas the pure graphene only shows a lower specific capacitance of 10.1 F/g at 10 mV/s. The results indicate that the prepared lignosulfonate−graphene composites have higher specific capacitance value implying excellent electrochemical performance. The effect of lignosulfonate mass loading on the electrochemical performance of the corresponding electrodes was measured by varying the concentration of lignosulfonate during the deposition process. The electrochemical performances of electrodes prepared in lignosulfonate with concentrations of 3, 10, 20, and 50 mg/mL were evaluated individually (Figure 4a−d) and showed that the capacitance reduced as the lignosulfonate concentration increased. With higher concentrations, thicker lignin will be incorporated on the graphene surface, but due to the insulating nature of lignosulfonate, the top layer lignin would have no contribution to the electron storage. By balancing the two competing factors, an optimum capacitance results. Figure 4e shows the CV curves of these four samples at the same scan rate of 20 mV/s. The peak current normalized to mass is decreased with higher concentration. As the thickness of lignosulfonate adsorbed on the wrinkling surface of graphene increases, relatively less active materials are used for energy storage, and therefore, the specific capacitance decreases.[1]

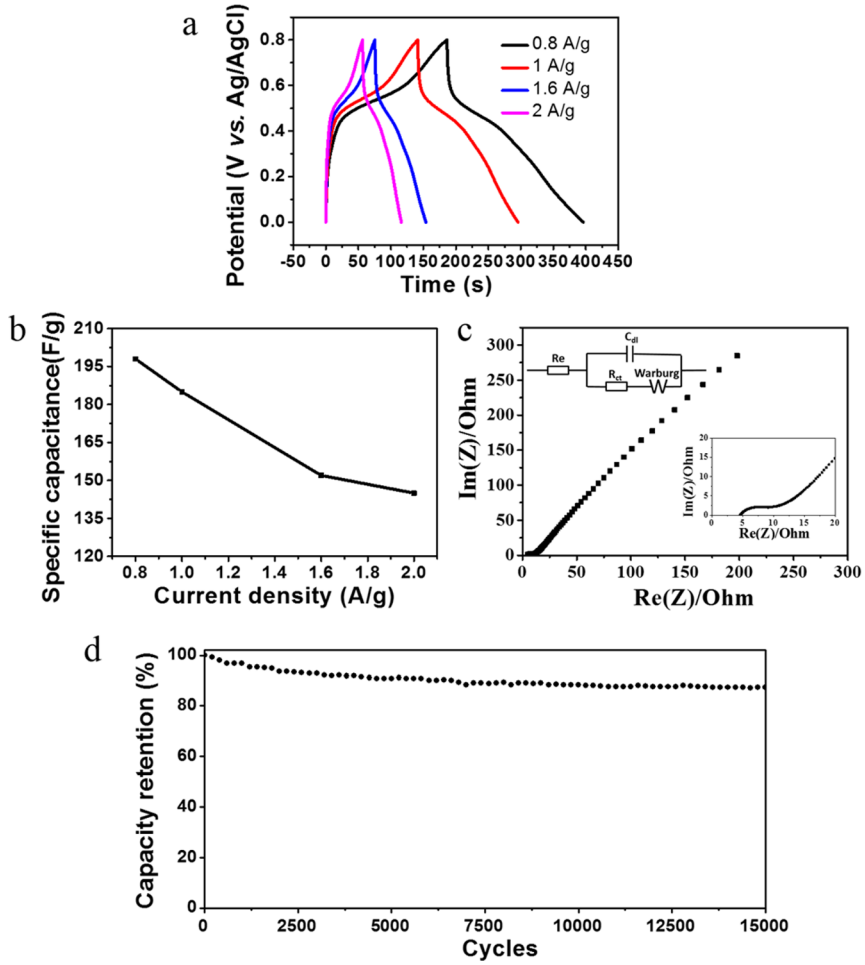

Figure 5. Electrochemical performance of lignosulfonate wrapped by graphene. (a) Galvanostatic charge−discharge profile of graphene−lignosulfonate prepared with 3 mg/mL concentration under different current densities. (b) Specific capacitance versus current density. (c) Electrochemical impedance curve of 3 mg/mL sample. (inset) Close-up image of the semicircle. (d) Cycling stability at a scan rate 2.0 A/g.

DOI: 10.1021/acssuschemeng.7b00322
ACS Sustainable Chem. Eng. XXXX, XXX, XXX−XXX

To further elucidate the electrochemical performance, galvanostatic charging and discharging of the lignosulfonate was conducted, as shown in Figure 5a. Here, we use a 3 mg/mL sample as an example. Elemental combustion analysis and thermogravimetric analysis were employed to detect the ratio of lignin and graphene in this hybrid electrode (Figure S4,). The charge−discharge curves at different current densities (0.8−2.0 A/g) between 0.1 and 0.8 V display different shapes compared to traditional capacitive ion storage, as there are Faradaic reactions happening in the presence of lignosulfonate. The curves look nearly symmetrical indicating a remarkable charge storing ability of this composites. The specific capacitances of the lignosulfonate are 226, 211, 174, and 166 F/g at current densities of 0.8, 1.0, 1.6, and 2.0 A/g, respectively (Figure 5b). The capacitance is only reduced by 26% as the current density increased from 0.8 to 2.0 A/g, which suggests excellent rate performance ascribed to the superior ion and electron transfer kinetics in this electrode. A previous report[15] on the electrochemical performance of polymer polypyrrole (lignosulfonate−anthraquinone sulfonate; Ppy(Lig-AQS)) electrode showed a discharge capacities around 186 mA h/g yielding a specific capacitance of 669.9 F/g at a current density of 1 A/g. In comparison, the specific capacitance of Ppy(Lig-AQS) is far higher than that of our prepared graphene-lignosulfonate electrode (211 F/g capacitance at a current density of 1.0 A/g), which may be attributed to the contribution capacitances from Ppy, Lig, and AQS.

To gain further insight into the superior kinetic performance of the lignosulfonate, electrical impedance spectroscopy (EIS) is measured and analyzed with the complex nonlinear least-squares (CNLS) fitting method on the basis of the equivalent circuit including a combined resistance R_e (ionic resistance of electrolyte, intrinsic resistance of electrode, and contact resistance at the active material/current collector interface) and a charge-transfer R_{ct} at the lignin and electrolyte interface, which is in serial connection with the Warburg resistance (W) and C_{dl} presenting the double-layer capacitance (inset of Figure 5c).[38] The Warburg resistance is a result of the frequency dependence of ion diffusion/transport in the electrolyte to the electrode surface. The Nyquist plot's (Figure 5c) first intercept value on the X-axis at high frequency, R_e, is 4 Ω, from which we can see the combined resistance is small implying high electrical conductivity. The R_{ct} obtained from the high frequency semicircle is around 5 Ω, which reveals a good charge transfer kinetic between the electrolyte and lignin. The Warburg region is very short, which indicates excellent electrolyte ion diffusion efficiency. Excellent cycling stability of the lignosulfonate electrode is obtained (Figure 5d), which shows that the mixed electrode measured at a current density of 2.0 A/g retains about 88%, of initial capacitance after 15 000 cycles. This cycle performance is far better than that of Ppy(Lig-AQS) (88% retention after 200 cycles), demonstrating the good stability of the graphene−lignosulfonate electrode.[15]

The excellent performance of the lignosulfonate is mainly due to their unique structural features. First, the reconfigurable graphene could act as microreactors and restrict the active material within the graphene cage; therefore, it could inhibit the loss of soluble active material. Meanwhile, highly conductive graphene facilitated the charge-transfer reaction by providing efficient electron transport pathways. Additionally, the flexible and porous graphene could work as buffers that provided strain relaxation and volume change accommodation. Its inner porous structure also offers easy access of the electrolyte to active nanoparticles, which increase the transfer efficiency of ions.

CONCLUSION

In summary, inspired by the venus flytrap, we capture and confine lignin as an electrochemically active species with a reconfigurable graphene, which is both an excellent electronic conductor and robust physical barrier against electrolyte dissolution. This biomimicry simultaneously resolves the poor electronic conductivity and high solubility of lignin in many electrolyte solutions. The encapsulation strategy developed here enables electrochemical energy storage devices with excellent rate capability and an exceptionally long lifespan. The lignin sandwiched between "graphene-flytrap" leaves delivers a high capacitance of 211 F/g at 1.0 A/g with stable performance of 15 000 cycles and 88% capacity retention. This strategy paves an avenue to eliminate the long-term cycling difficulty for lignin-based electrode materials and enables the feasible conversion of lignin into a sustainable and low-cost energy storage material.

EXPERIMENTAL SECTION

Materials. Technical soda bagasse lignin with 3.41% moisture content was provided from Granit Corp. (Lausanne, Switzerland). Lignosulfonate was provided by Aditya Brilas Mill Domsjö Fabriker, Sweden. Graphite (99.8%) and H_2O_2 (30%) were purchased from Sigma-Aldrich. Anhydrous ferric chloride powders were purchased from Fisher Scientific.

Sample Preparation. Ferric chloride-graphite intercalation compounds (GIC) were synthesized via a conventional two-zone vapor transport technique.[37,39] Natural graphite flakes and anhydrous ferric chloride powders were placed separately in a two-zone reactive container and then sealed. All these procedures were operated in a nitrogen filled glovebox (H_2O < 1 ppm and O_2 < 1 ppm). The mixture was then heated at 360 °C for 24 h in a furnace. As-synthesized $FeCl_3$-intercalated graphite and H_2O_2 (30%) were loaded into a reactive bottle at room temperature for 10 h. The graphite was exfoliated into long flytrap-like graphite which was composed of interconnected graphene layers.

The GIC was immersed in hydrogen peroxide solution for 24 h to open the wrinkling surface by Fenton reaction. The flytrap-like GIC was then washed by ethanol and deionized water three times respectively after being digested by hydrochloric acid to the residual ferric ion. Next, the flytrap-like GIC was saturated in lignosulfonate solution for 24 h. Finally, the GIC-lignin composites were dried at room temperature.

Sample Characterization. *Nuclear Magnetic Resonance (NMR) Spectroscopy.* All NMR measurements were acquired at 25 °C on a Bruker Avance III HD 400 MHz instrument. The probe head used was a 5 mm BBFO broadband probe equipped with a Z-gradient coil. The instrument had an automatic tuning and matching unit as well as an automatic shimming unit. The NMR sample was prepared by dissolving the Domsjö sodium lignosulfonate (100 mg) in the NMR solvent (D_2O, 700 μL), and then, the solution was transferred into a 5 mm NMR tube through a filter. The proton spectrum was acquired by using a spectral window of 20 ppm, 64 000 data points in the time domain, an acquisition time of 4.09 s, a relaxation delay time of 1 s between each scan, and a total number of 16 scans. The ^{13}C NMR spectrum was acquired by using a spectral window of 239 ppm, 64 000 data points in the time domain, an acquisition time of 1.36 s, a relaxation delay time of 2 s between each scan, and a total number of 20 000 scans. The 2D HSQC NMR spectrum was acquired by using the Bruker pulse program "hsqcetgpsi", acquisition time 0.12 s, relaxation delay 0.82 s, a coupling constant of 145 Hz, an INEPT transfer delay time of 1.72 ms (d_4 = 1/4J), a spectral window of 10.5 ppm in $F2$ and 166 ppm in $F1$ with 1024 × 512 increments, 100 scans per increment, and a spectral center set at 90.0 ppm in $F1$ and 5.3 ppm

DOI: 10.1021/acssuschemeng.7b00322
ACS Sustainable Chem. Eng. XXXX, XXX, XXX−XXX

in *F2*. The 2D NMR data set was processed with 2000 × 1000 data points using a $\pi/2$ shifted sine bell window function in both dimensions.

Gel Permeation Chromatography (GPC) Analysis. Molecular weight distributions of the samples were investigated by dissolving 5 mg of lyophilized samples in 2 mL of DMSO + 0.5% LiBr (w/w) solution. After filtration of the samples through 0.45um PTFE filters, size exclusion chromatography (SEC) was performed with SEC 1260 Infinity (Polymer Standard Services, Germany). The equipment consisted of an isocratic pump (G1310B), a micro degasser (G1379B), and a standard autosampler (G1329B). The detection system included a UV detector (G1314B) in series with a refractive index detector (G1362A). The mobile phase was DMSO + 0.5% LiBr set to a constant flow rate of 0.5 mL/min for a total run time of 65 min. The injection volume was 100 μL. The separation system consisted of PSS GRAM Precolumn, PSS GRAM 100 Å, and PSS GRAM 10 000 Å analytical columns thermostated at 60 °C and connected in series. The pullulan standards with nominal masses of 708, 337, 194, 47.1, 21.1, 9.6, 6.1, 1.08, and 342 Da were used for standard calibration.

Scanning Electron Microscopy (SEM) Observations. A scanning electron microscope (Hitachi S4800) was used to characterize the surface morphology of GIC before and after saturation in lignosulfonate solution at a beam intensity of 5 kV. Elemental analysis was conducted by energy dispersive X-ray spectroscopy. The sample was prepared in liquid nitrogen to maintain the morphology well.

Thermogravimetric/Differential Thermal Analyzer (TG-DTA). The lignosulfonate mass was measured by thermogravimetric analysis. (TA Instruments SDT Analyzer Q600) The GIC-Lignin composites were dried at 105 °C for 4 h in an oven prior to testing. Then, all samples were decomposed at a temperature range of 100 to 1200 °C at a heating rate of 10 °C/min under nitrogen in TG-DTA.

X-ray Photoelectron Spectroscopy (XPS). XPS was conducted using an Axis Ultra DLD (Kratos) system. The chamber was at 1 × 10^{-9} Torr vacuum. A monochromatic aluminum Kα source with a source power of 150 W (15 kV × 10 mA) was used. The pass energy was 160 eV for wide scans and 40 eV for narrow scans.

Raman Spectroscopy. Raman spectroscopy was performed using a LabRam HR800 UV NIR and 532 nm laser excitation with working distances on a ×50 lens. The Raman spectra of M-MoS_2 and S-MoS_2 were recorded by depositing the samples on silicon substrates.

XRD Patterns. The XRD patterns of M-MoS_2 and S-MoS_2 were recorded for two theta values ranging from 4−18° to characterize the interlayer spacing. The characterization was performed on a Bruker AXS-D8 Advance powder X-ray diffractometer using Cu/Ka radiation (λ = 1.5406 Å) with a step size of 0.02° and a dwell time of 3.0 s.

Elemental Combustion Analysis. The total weight of active material in the working electrode was 0.5 mg. In addition, the working electrode was used without introducing any additional polymer binder or conductive additive. The instrument used was an ELTRA CS 500. For our samples, approximately 2−10 mg were weighed on a microbalance, loaded into a combustion boat, and then transferred into the combustion analyzer and combusted in an ultrapure oxygen environment. The generated gaseous products were analyzed by IR. Control standards were run before and after samples and were calibrated to be within acceptable limits.

Electrochemical Analysis. Electrochemical characterization was performed using a biological electrochemical station SP150 equipped with a three-electrode system, which was comprised of a platinum mesh working, a platinum foil counter, and Ag/AgCl reference electrodes. Cyclic voltammetry measurements were conducted in 0.1 M $HClO_4$ solution from 0 to 0.8 V at scan rates of 10, 20, 50, and 100 mV/s. Electrochemical impedance spectroscopy was conducted at a frequency range of 100 kHz to 0.01 Hz at the open circuit potential with 10 mV amplitude. Charging−discharging analysis was performed from 0.1 to 0.8 V at different current densities. All of the electrochemical experiments were carried out at room temperature.

■ ASSOCIATED CONTENT

Supporting Information

The Supporting Information is available free of charge on the ACS Publications website at DOI: 10.1021/acssuschemeng.7b00322.

NMR mapping signal, −OH group content, GPC analysis, SEM, CV, specific capacitance, and TG-DTA (PDF)

■ AUTHOR INFORMATION

Corresponding Author

*E-mail: h.zhu@neu.edu (H.Z.).

ORCID

Hongli Zhu: 0000-0003-1733-4333

Author Contributions

§X.G., Y.Z., and L.J. contributed equally to this work.

Notes

The authors declare no competing financial interest.

■ ACKNOWLEDGMENTS

H.Z. acknowledges the financial startup support and Tier 1 support from Northeastern University. We thank Suzhou Graphene Nanotechnology Co., Ltd, for providing the GIC and graphite. We thank Wei Wen for helping with schematic drawing. We also thank the Center for Nanoscale System (CNS) at Harvard University for the use of their facilities.

■ REFERENCES

(1) Milczarek, G.; Inganäs, O. Renewable Cathode Materials from Biopolymer/Conjugated Polymer Interpenetrating Networks. *Science* **2012**, *335* (6075), 1468−1471.

(2) Azadi, P.; Inderwildi, O. R.; Farnood, R.; King, D. A. Liquid fuels, hydrogen and chemicals from lignin: A critical review. *Renewable Sustainable Energy Rev.* **2013**, *21*, 506−523.

(3) Dolgonosov, B.; Gubernatorova, T. Modeling the biodegradation of multicomponent organic matter in an aquatic environment: 2. Analysis of the structural organization of lignin. *Water Resour.* **2010**, *37* (3), 320−331.

(4) Zhu, H.; Areskogh, D.; Helander, M.; Henriksson, G. Investigation on enzymatic oxidative polymerization of technical soda lignin. *Curr. Org. Chem.* **2012**, *16* (16), 1850−1854.

(5) Zhu, H.; Li, Y.; Pettersson, B.; Zhang, L.; Lindström, M.; Henriksson, G. Technical soda lignin dissolved in urea as an environmental friendly binder in wood fiberboard. *J. Adhes. Sci. Technol.* **2014**, *28* (5), 490−498.

(6) Berlin, A.; Balakshin, M. *Industrial lignins: analysis, properties and applications*; Elsevier: Amsterdam, 2014; pp 315−336.

(7) Janshekar, H.; Fiechter, A. Lignin: biosynthesis, application, and biodegradation. In *Pentoses and Lignin*; Springer, 1983; pp 119−178.

(8) Zhang, X.; Tu, M.; Paice, M. G. Routes to potential bioproducts from lignocellulosic biomass lignin and hemicelluloses. *BioEnergy Res.* **2011**, *4* (4), 246−257.

(9) Varanasi, P.; Singh, P.; Auer, M.; Adams, P. D.; Simmons, B. A.; Singh, S. Survey of renewable chemicals produced from lignocellulosic biomass during ionic liquid pretreatment. *Biotechnol. Biofuels* **2013**, *6*, 14−14.

(10) Ragauskas, A. J.; Beckham, G. T.; Biddy, M. J.; Chandra, R. P.; Chen, F.; Davis, M. F.; Davison, B. H.; Dixon, R. A.; Gilna, P.; Keller, M.; et al. Lignin Valorization: Improving Lignin Processing in the Biorefinery. *Science* **2014**, *344* (6185), 1246843−1246843.

(11) Tenhaeff, W. E.; Rios, O.; More, K.; McGuire, M. A. Highly Robust Lithium Ion Battery Anodes from Lignin: An Abundant, Renewable, and Low-Cost Material. *Adv. Funct. Mater.* **2014**, *24* (1), 86−94.

DOI: 10.1021/acssuschemeng.7b00322
ACS Sustainable Chem. Eng. XXXX, XXX, XXX−XXX

(12) Kadla, J.; Kubo, S.; Venditti, R.; Gilbert, R.; Compere, A.; Griffith, W. Lignin-based carbon fibers for composite fiber applications. *Carbon* **2002**, *40* (15), 2913−2920.
(13) Chen, T.; Zhang, Q.; Xu, J.; Pan, J.; Cheng, Y.-T. Binder-free lithium ion battery electrodes made of silicon and pyrolized lignin. *RSC Adv.* **2016**, *6* (35), 29308−29313.
(14) Wang, S.-X.; Yang, L.; Stubbs, L. P.; Li, X.; He, C. Lignin-derived fused electrospun carbon fibrous mats as high performance anode materials for lithium ion batteries. *ACS Appl. Mater. Interfaces* **2013**, *5* (23), 12275−12282.
(15) Nagaraju, D. H.; Rebis, T.; Gabrielsson, R.; Elfwing, A.; Milczarek, G.; Inganas, O. Charge Storage Capacity of Renewable Biopolymer/Conjugated Polymer Interpenetrating Networks Enhanced by Electroactive Dopants. *Adv. Energy Mater.* **2014**, *4* (1), 1300443.
(16) Gnedenkov, S. V.; Opra, D. P.; Zemnukhova, L. A.; Sinebryukhov, S. L.; Kedrinskii, I. A.; Patrusheva, O. V.; Sergienko, V. I. Electrochemical performance of Klason lignin as a low-cost cathode-active material for primary lithium battery. *J. Energy Chem.* **2015**, *24* (3), 346−352.
(17) Gnedenkov, S. V.; Opra, D. P.; Sinebryukhov, S. L.; Tsvetnikov, A. K.; Ustinov, A. Y.; Sergienko, V. I. Hydrolysis lignin-based organic electrode material for primary lithium batteries. *J. Solid State Electrochem.* **2013**, *17* (10), 2611−2621.
(18) Popova, O. V.; Popova, S. S.; Ol'shanskaya, L. N. O. Prospects for using artificial graphite produced from lignin in electrodes of chemical power cells. *Russ. J. Appl. Chem.* **2008**, *81* (5), 786−791.
(19) Balandin, A. A.; Ghosh, S.; Bao, W. Z.; Calizo, I.; Teweldebrhan, D.; Miao, F.; Lau, C. N. Superior thermal conductivity of single-layer graphene. *Nano Lett.* **2008**, *8* (3), 902−907.
(20) Novoselov, K. S.; Geim, A. K.; Morozov, S. V.; Jiang, D.; Katsnelson, M. I.; Grigorieva, I. V.; Dubonos, S. V.; Firsov, A. A. Two-dimensional gas of massless Dirac fermions in graphene. *Nature* **2005**, *438* (7065), 197−200.
(21) Novoselov, K. S.; Geim, A. K.; Morozov, S. V.; Jiang, D.; Zhang, Y.; Dubonos, S. V.; Grigorieva, I. V.; Firsov, A. A. Electric field effect in atomically thin carbon films. *Science* **2004**, *306* (5696), 666−669.
(22) Novoselov, K. S.; Jiang, Z.; Zhang, Y.; Morozov, S. V.; Stormer, H. L.; Zeitler, U.; Maan, J. C.; Boebinger, G. S.; Kim, P.; Geim, A. K. Room-temperature quantum hall effect in graphene. *Science* **2007**, *315* (5817), 1379−1379.
(23) Schedin, F.; Geim, A. K.; Morozov, S. V.; Hill, E. W.; Blake, P.; Katsnelson, M. I.; Novoselov, K. S. Detection of individual gas molecules adsorbed on graphene. *Nat. Mater.* **2007**, *6* (9), 652−655.
(24) Tombros, N.; Jozsa, C.; Popinciuc, M.; Jonkman, H. T.; van Wees, B. J. Electronic spin transport and spin precession in single graphene layers at room temperature. *Nature* **2007**, *448* (7153), 571−574.
(25) Geng, X.; Guo, Y.; Li, D.; Li, W.; Zhu, C.; Wei, X.; Chen, M.; Gao, S.; Qiu, S.; Gong, Y.; Wu, L.; Long, M.; Sun, M.; Pan, G.; Liu, L. Interlayer catalytic exfoliation realizing scalable production of large-size pristine few-layer graphene. *Sci. Rep.* **2013**, *3*, 1134.
(26) Ralph, J.; Marita, J. M.; Ralph, S. A.; Hatfield, R. D.; Lu, F.; Ede, R. M.; Peng, J.; Landucci, L. L. Solution state NMR of lignins. *Advances in lignocellulosics characterization*; TAPPI: Atlanta, GA, 1999.
(27) Wen, J. L.; Sun, S. L.; Xue, B. L.; Sun, R. C. Recent Advances in Characterization of Lignin Polymer by Solution-State Nuclear Magnetic Resonance (NMR) Methodology. *Materials* **2013**, *6* (1), 359−391.
(28) Lutnaes, B. F.; Myrvold, B. O.; Lauten, R. A.; Endeshaw, M. M. 1H and 13C NMR data of benzylsulfonic acids—model compounds for lignosulfonate. *Magn. Reson. Chem.* **2008**, *46* (3), 299−305.
(29) Madad, N.; Chebil, L.; Sanchez, C.; Ghoul, M. Effect of molecular weight distribution on chemical, structural and physicochemical properties of sodium lignosulfonates. *RASAYAN J. Chem.* **2011**, *4*, 189−202.
(30) Choucair, M.; Thordarson, P.; Stride, J. A. Gram-scale production of graphene based on solvothermal synthesis and sonication. *Nat. Nanotechnol.* **2009**, *4* (1), 30−33.
(31) Gomez-Navarro, C.; Weitz, R. T.; Bittner, A. M.; Scolari, M.; Mews, A.; Burghard, M.; Kern, K. Electronic transport properties of individual chemically reduced graphene oxide sheets. *Nano Lett.* **2007**, *7* (11), 3499−3503.
(32) Kudin, K. N.; Ozbas, B.; Schniepp, H. C.; Prud'homme, R. K.; Aksay, I. A.; Car, R. Raman spectra of graphite oxide and functionalized graphene sheets. *Nano Lett.* **2008**, *8* (1), 36−41.
(33) Stankovich, S.; Dikin, D. A.; Piner, R. D.; Kohlhaas, K. A.; Kleinhammes, A.; Jia, Y.; Wu, Y.; Nguyen, S. T.; Ruoff, R. S. Synthesis of graphene-based nanosheets via chemical reduction of exfoliated graphite oxide. *Carbon* **2007**, *45* (7), 1558−1565.
(34) Tung, V. C.; Allen, M. J.; Yang, Y.; Kaner, R. B. High-throughput solution processing of large-scale graphene. *Nat. Nanotechnol.* **2009**, *4* (1), 25−29.
(35) Underhill, C.; Leung, S. Y.; Dresselhaus, G.; Dresselhaus, M. S. Infrared and Raman-Spectroscopy of Graphite-Ferric Chloride. *Solid State Commun.* **1979**, *29* (11), 769−774.
(36) Li, B.; Zhou, L.; Wu, D.; Peng, H. L.; Yan, K.; Zhou, Y.; Liu, Z. F. Photochemical Chlorination of Graphene. *ACS Nano* **2011**, *5* (7), 5957−5961.
(37) Geng, X. M.; Guo, Y. F.; Li, D. F.; Li, W. W.; Zhu, C.; Wei, X. F.; Chen, M. L.; Gao, S.; Qiu, S. Q.; Gong, Y. P.; Wu, L. Q.; Long, M. S.; Sun, M. T.; Pan, G. B.; Liu, L. W. Interlayer catalytic exfoliation realizing scalable production of large-size pristine few-layer graphene. *Sci. Rep.* **2013**, DOI: 10.1038/srep01134.
(38) Chen, X.; Zhu, H.; Chen, Y.-C.; Shang, Y.; Cao, A.; Hu, L.; Rubloff, G. W. MWCNT/V2O5 Core/Shell Sponge for High Areal Capacity and Power Density Li-Ion Cathodes. *ACS Nano* **2012**, *6* (9), 7948−7955.
(39) Zhao, W. J.; Tan, P. H.; Liu, J.; Ferrari, A. C. Intercalation of Few-Layer Graphite Flakes with FeCl3: Raman Determination of Fermi Level, Layer by Layer Decoupling, and Stability. *J. Am. Chem. Soc.* **2011**, *133* (15), 5941−5946.

DOI: 10.1021/acssuschemeng.7b00322
ACS Sustainable Chem. Eng. XXXX, XXX, XXX−XXX